Materials Advances

ROYAL SOCIETY OF CHEMISTRY

PAPER

View Article Online
View Journal | View Issue

Check for updates

Cite this: *Mater. Adv.*, 2024, **5**, 7230

Vapor selective and controlled actuation of gelatin-based soft actuators†

Vipin Kumar,[ab] Sarah Ahmad Siraj[ab] and Dillip K. Satapathy *[ab]

Biopolymer-based soft actuators, responsive to vapor stimuli, show promise in the fields of soft robotics, smart textiles, and energy harvesting, effectively addressing the limitations of their synthetic polymer-based counterparts while offering advantages in biocompatibility and sustainability. We report rapid and fully reversible actuation characteristics of biopolymer gelatin-based soft actuators upon exposure to water and ethanol vapors. The repeatability of the actuation performance is established *via* extensive testing involving over 1200 vapor exposure cycles. Notably, these gelatin-based actuators display distinct responses to water and ethanol vapors. For instance, they bend upwards in water vapor and downward in ethanol vapor. By tuning the ratio of water to ethanol vapor in binary solutions, the magnitude and direction (upward or downward) of the actuation of the gelatin films can be precisely controlled. The actuation performance of gelatin film is fine-tuned with added salts and saccharides, while also exploring the effects of crystalline structure and post-annealing procedures on its properties. Furthermore, the tunability of the bending axis of the soft actuator is achieved by imprinting oriented periodic patterns onto the surface of the gelatin films. These periodic patterns not only enhance the actuation performance significantly but also aid in generating rectilinear motion of these gelatin film-based actuators. The gelatin-based soft actuators produce a lifting force of around 7 millinewtons when exposed to water vapor and can lift approximately 25 times their weight in response to ethanol vapor. Leveraging the unique vapor-responsive characteristics of the gelatin film, several proof-of-concept applications, including ethanol vapor sensors, intelligent curtains, adaptive lifts, wave-like motion, and voltage generation systems, are demonstrated.

Received 6th January 2024,
Accepted 31st July 2024

DOI: 10.1039/d4ma00015c

rsc.li/materials-advances

Open Access Article. Published on 05 August 2024. Downloaded on 2/21/2026 9:32:34 AM.
This article is licensed under a Creative Commons Attribution-NonCommercial 3.0 Unported Licence.

1. Introduction

Drawing inspiration from the remarkable abilities displayed in nature, such as opening and closing of Mimosa pudica plant leaves[1] and adaptation of pine cone scales,[2] researchers increasingly turn to nature for insights into designing soft actuators.[3] Soft actuators, a revolutionary class of materials for advancing soft robotics, leverage the intrinsic properties of soft, flexible, and compliant materials to generate versatile movements, unlike traditional rigid actuators relying on mechanical systems and motors.[3] Soft actuators that adapt to different environments have gained significant attention due to their unique applications in the manipulation of delicate objects (soft grippers), artificial muscles,[4] biomedical applications,[5] smart textiles,[6] energy harvesting devices,[7] and biomimicry.[8] These soft actuators are made up of polymers,[9,10] hydrogels,[11,12] and liquid crystals,[13] and undergo controlled shape changes in response to various external stimuli like light,[14] temperature,[15] humidity,[9,16] electric[17] and magnetic[18] fields, chemical vapors,[19,20] *etc.* While soft actuators triggered by stimuli such as light, heat, electric, and magnetic fields have been extensively studied, studies on soft actuators that respond to solvent vapors are relatively scarce. These vapor-responsive soft actuators offer distinct advantages compared to their counterparts, presenting innovative mechanisms for achieving substantial shape transformations and locomotion. By drawing from principles grounded in solvent diffusion and fluid mechanics, vapor-responsive soft actuators exhibit precise and rapid responses to changes in vapor concentration levels. Notably, when the stimulus is water vapor, the advantages of these

[a] *Soft Materials Laboratory, Department of Physics, IIT Madras, Chennai-600036, Tamil Nadu, India. E-mail: dks@iitm.ac.in*
[b] *Center for Soft and Biological Matter, IIT Madras, Chennai-600036, Tamil Nadu, India*

† Electronic supplementary information (ESI) available: The ESI contains TGA and DSC of the gelatin film, tensile testing plot, maximum bending curvature of the gelatin film upon exposure to water at different environmental humidities, effect of the water source temperature on the actuation, bending curvature in response to different alcohol vapors, the basic molecular structure of the gelatin, swelling of the gelatin film in water, desiccation effect plot, weight change plot of the gelatin film in ethanol vapor, X-ray diffraction pattern recorded for the gelatin films dried at 28 ± 1 °C and 40 ± 1 °C, the temporal evolution of the bending curvature of the smooth (black) and patterned (red) film, snapshots of the square-shaped non-patterned and patterned gelatin film upon water vapor exposure, the weight-lifting capacity of the gelatin film, and actuation properties comparison table. (PDF). See DOI: https://doi.org/10.1039/d4ma00015c

© 2024 The Author(s). Published by the Royal Society of Chemistry

Open Access Article. Published on 05 August 2024. Downloaded on 2/21/2026 9:32:34 AM. This article is licensed under a Creative Commons Attribution-NonCommercial 3.0 Unported Licence.

actuators are significantly enhanced due to the ubiquitous presence of water and its biocompatibility.

The physics of the actuation process of vapor-driven soft actuators is primarily based on the expansion and contraction of materials in the presence of a vapor stimulus. Some synthetic polymers (PVA,[21] PVDF,[22] PDMS,[20] nanomaterials[23,24]), and natural (silk,[16] cellulose,[25] starch,[23] and gelatin[26]) materials have been used to design vapor responsive actuators. The introduction of synthetic or rigid materials into soft actuators introduces complexity and has serious implications for biocompatible applications. Furthermore, achieving seamless integration of essential features within soft actuators to ensure their optimal performance and adaptability is of paramount importance. Therefore, it is advantageous to create soft actuators using environment friendly, single-phase materials without any additives. It is crucial to consider the following factors for achieving optimal soft actuator performance in natural polymers – (i) availability of the appropriate functional groups for interaction with vapor stimuli; (ii) the imperative incorporation of biocompatible materials; underlining the importance of safe and non-toxic interactions between soft actuators and biological systems; (iii) stability in actuation performance over multiple cycles ensuring reliability and durability in various applications; and (iv) precise control of magnitude and actuation direction.

Soft actuators based on biopolymers are attracting significant attention that fulfills the aforementioned essential features for achieving optimal actuation. These bio-polymer actuators respond to liquid solvents or vapors and find potential applications in areas like artificial muscles,[27] and wearable electronics.[28,29] Conventional vapor-responsive soft actuators use bilayers of different biopolymers that expand differently with exposure to vapor.[30] However, a major drawback is poor compatibility between the polymers at their interfaces, leading to delamination during repeated actuation cycles. To address these challenges, single-layer vapor-responsive soft actuators are explored. One such example is the work of Ze Zhao *et al.*,[31] where they designed a single-layer actuator using pollen grains. This actuator exhibits responsiveness solely to water vapor as an external stimulus, and repeatability is limited to only a few tens of cycles. To enhance the actuation performance, various inorganic materials, such as graphene oxide and MXene, have been incorporated into bio-polymers. For instance, Chathuranga Hiran *et al.*[32] integrated graphene oxide into a starch-based bio-polymer film, improving the mechanical properties. Similarly, when MXene is mixed with cellulose, it increases the complexity of the system and degrades the bio-compatibility of the resulting actuator.[6] However, it is worth noting that incorporating graphene oxide, MXene, and other organic materials impacts the cost, bio-compatibility, bio-degradability, and complexity of the actuator system. To tackle these challenges comprehensively, we propose a single-layer vapor-responsive soft actuator based on biopolymer gelatin without any additives. Gelatin is a protein derived from collagen hydrolysis, sourced from animal connective tissues like bones, skin, and tendons.[33] It is known for being odorless, tasteless, and widely used in the food and pharmaceutical industries as a gelling agent and thickener. The chemical structure of gelatin primarily consists of a long chain of amino acids, forming a polypeptide with a repeating sequence of these amino acids.[34,35] A basic amino acid molecule contains a central carbon (α-carbon) bonded to hydrogen, an amino group ($-NH_2$), a carboxyl group (–COOH) and an R group, and a unique amino acid side chain that distinguishes one amino acid from another and due to the presence of amino acids, gelatin shows a hydrophilic nature and absorbs large amounts of water.[36] It is worth mentioning that gelatin-based vapor-responsive soft actuators without any additives remain unexplored. Most existing studies on soft actuators made from gelatin usually revolve around composite materials mixed with various additives. For example, Yonghao Liu *et al.*[26] reported a composite film of gelatin with PEDOT:PSS, which responds to only water vapor. In another study, Yang *et al.*[37] reported temperature-triggered shape memory hydrogel prepared by soaking gelatin gel in tannic acid. Huang *et al.*[38] designed a NIR-light triggered actuator based on a hydrogel composed of polyacrylamide–GO–gelatin polymer. Similarly, Zhu *et al.*[39] reported a self-healing, multiple-responsive hydrogel composed of gelatin/PAAm/Clay for sensing applications. Observations have been made regarding using gelatin in the soft actuator domain as a hydrogel and in composite structures. Nevertheless, there is a lack of reports on pristine gelatin-based single-layer soft actuators with vapor selective and controlled actuation.

This work demonstrates novel vapor-selective actuation characteristics of gelatin-based single-layer soft actuators without any additives. The actuation performance is tuned by adding salt and sugar into the gelatin film, varying the crystalline structure of the film, and subjecting it to post-annealing. Additionally, we introduce a simple method to pattern the surface of the gelatin film, improving actuation performance by 95% and enabling manipulation of the bending axis for diverse applications. This surface patterning not only controls the bending axis but also converts random locomotion into linear motion. Furthermore, these actuators display unique vapor selective actuation in response to water and ethanol vapors, offering precise control over the actuation magnitude. By vapor selectivity, our mean is that the gelatin film exhibits vapor selectivity by distinguishing between water and alcohol vapors. They maintain remarkable stability and repeatability, even after more than 1200 actuation cycles, meeting crucial criteria for practical applications. These gelatin-based single-layer soft actuators are fabricated *via* a facile solution-casting method, which preserves the bio-compatibility and biodegradability properties of the gelatin. We demonstrate the utility of these soft actuators in various applications, including ethanol vapor sensors, smart lifts, smart curtains, wave-like undulating structures, and voltage generation capabilities, showcasing their versatility.

2. Experimental methods

The primary ingredient, a pale yellow powder form of gelatin (Type A, 175 Bloom), was obtained from Alfa Aesar. The food color used in this work was purchased from Papilon, Magic Flairs, India. Salt (NaCl) and sugar (sucrose) were purchased

Open Access Article. Published on 05 August 2024. Downloaded on 2/21/2026 9:32:34 AM.
This article is licensed under a Creative Commons Attribution-NonCommercial 3.0 Unported Licence.

from Merck and used as received. The piezo PVDF film with screen-printed silver electrodes, 28 μm thick, was purchased from PolyK Technologies, USA. Millipore ultra-pure water with a resistivity of 18.2 MΩ cm was used to prepare the gelatin solution. Ethanol (99%) was used in its undiluted form as a vapor source.

2.1. Preparation of gelatin film

Gelatin-based soft actuators were fabricated using a facile solution-casting method, and the synthesis protocol is schematically depicted in Fig. 1(a). A transparent solution containing 3 wt% of gelatin in Millipore ultra-pure water is prepared. The mixture was stirred on a hot plate set at 90 °C and 400 rpm until complete dissolution was achieved. To aid the visibility of the film in an optical camera, a minute quantity of red food color (Papilon) was added to the solution. The colored gelatin solution was poured into a polystyrene petri dish with a smooth surface and left to dry under ambient atmospheric conditions (30 °C and 60% RH). After complete drying, the resulting free-standing gelatin films were carefully peeled off and stored in a desiccator for further use. To see the effect of crystalline structure on the actuation characteristics, films with different crystalline structures were prepared by drying the gelatin solution at different temperatures, such as 28 °C and 40 °C under 60% relative humidity conditions. A similar protocol was followed to prepare the gelatin films with the addition of salt (NaCl, 2.5 and 5 wt% of dry gelatin powder) and sugar (sucrose, 5 and 10 wt% of dry gelatin powder).

2.2. Preparation of patterned gelatin film

To fabricate gelatin film with patterned surfaces, 3 wt% gelatin solution was directly poured onto a grooved polypropylene substrate with grooves measuring 28 μm in height and 100 μm in width with 2 mm separation. After the complete evaporation of water, the patterned gelatin films were carefully peeled off from the substrate and stored in a desiccator for further experiments.

2.3. Characterizations

The molecular structure of the prepared gelatin films was confirmed by the Fourier transfer infrared spectroscopy in attenuated total reflection (ATR) mode by FTIR (PerkinElmer) in the frequency range 4000–400 cm^{-1}. X-ray diffraction data were collected using an Aeris Benchtop X-Ray Diffractometer

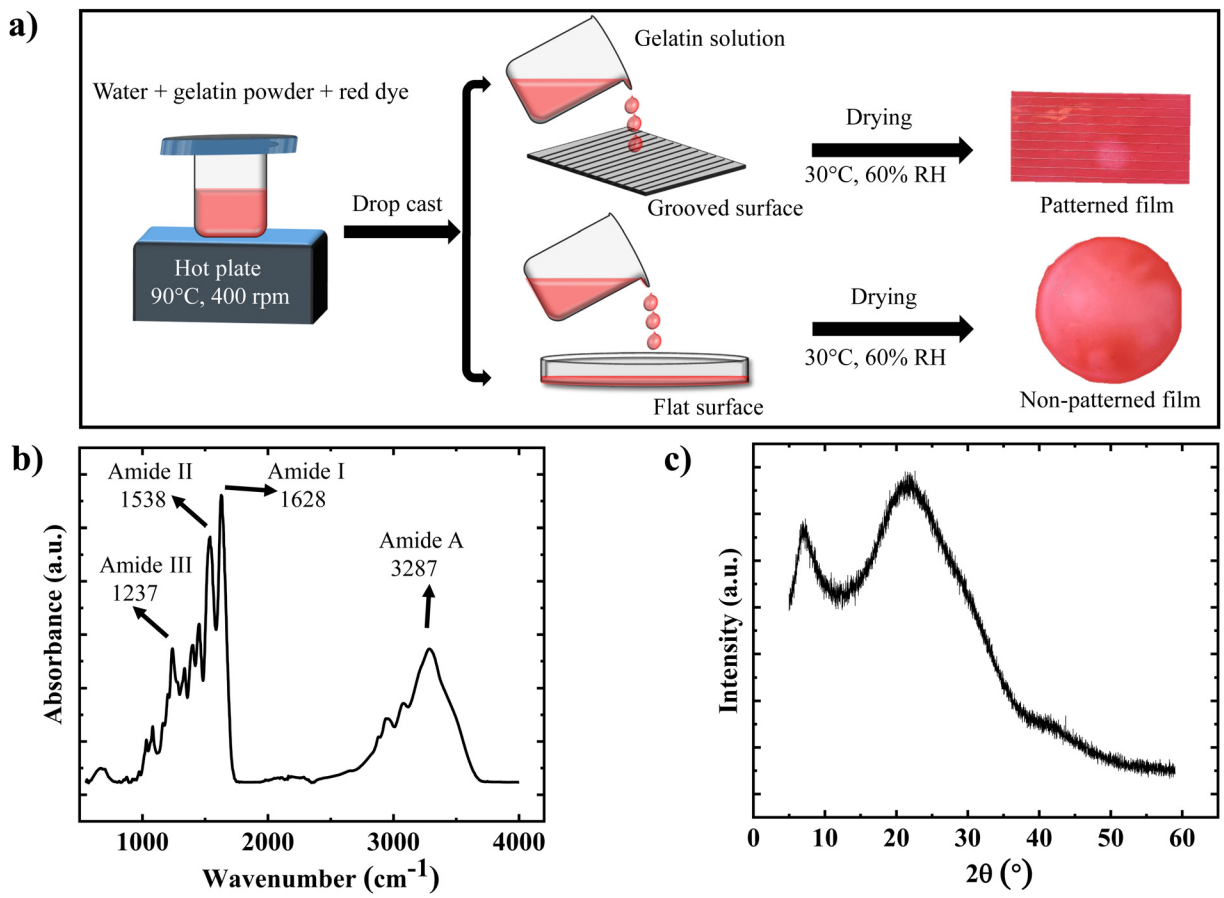

Fig. 1 (a) The preparation method of gelatin film with a patterned and smooth surface illustrated schematically. The gelatin solution was poured on the smooth and grooved surface and left for drying. After complete evaporation of water, the film was carefully peeled off. (b) ATR-FTIR spectra of the gelatin film and peaks are marked to correspond to different bonds present in the film. FTIR spectra confirm the presence of hydrophilic groups in the gelatin film. (c) An X-ray diffraction pattern was recorded for the gelatin film, showing the semi-crystalline nature of the film.

© 2024 The Author(s). Published by the Royal Society of Chemistry

Open Access Article. Published on 05 August 2024. Downloaded on 2/21/2026 9:32:34 AM. This article is licensed under a Creative Commons Attribution-NonCommercial 3.0 Unported Licence.

(PANalytical) with Cu Kα radiation in the diffraction angle range $2\theta = 5^\circ$ to $2\theta = 60^\circ$. The thermal properties of the gelatin film were measured by differential scanning calorimetry (DSC) and thermogravimetric analysis (TGA). TGA of the gelatin film was performed in the temperature range of 25–500 °C with a rate of 10 °C min^{-1} in an argon atmosphere with a flow rate of 100 mL min^{-1}. DSC of the gelatin film was conducted in the temperature range 30–150 °C with a rate of 10 °C min^{-1} in an argon atmosphere with a flow rate of 100 mL min^{-1}. The mechanical properties of the gelatin film were measured by the Instron 5948 tensile testing machine. The gauge length was kept at 30 mm, and the extension rate was 2 mm min^{-1}. The mechanical testing was performed at room temperature (25 °C) and relative humidity 45%.

3. Results and discussion

3.1. Preparation and characterization of the gelatin film

The patterned and non-patterned gelatin films are prepared by following a solution-casting method and are schematically displayed in Fig. 1(a) (details are given in the Experimental methods). The FTIR spectra of the gelatin film are displayed in Fig. 1(b), where the characteristics peak at 3287 cm^{-1} represents the stretching of N–H and O–H (amide A region), 1628 cm^{-1} represents the C═O stretching (amide I), 1539 cm^{-1} represents the bending of N–H and stretching of C–N vibrations (amide II), and 1239 cm^{-1} represents the N–H bending (amide III).[40,41] The X-ray diffraction pattern depicted in Fig. 1(c) confirms the crystalline nature of the prepared gelatin film. The sharp peak observed at $2\theta = 7^\circ$ corresponds to the diameter of the triple helix, and its intensity correlates with the triple-helix content in the film. Additionally, the second broad peak at $2\theta = 21^\circ$ corresponds to the distance between amino acid residues.[42–44] The two stages of weight loss upon increase in temperature are revealed *via* TGA measurement (Fig. S1(a), ESI†). The first stage (50 °C to 100 °C) is attributed to the loss of free and bound water inherent in gelatin due to its highly hygroscopic nature. The second weight-loss stage (250 °C to 450 °C) corresponds to the thermal degradation of the proteins within the gelatin film.[45,46] The DSC plot (Fig. S1(b), ESI†) provided the glass transition and melting temperatures of the gelatin films dried at two different temperatures. Two transition peaks were observed: the first representing the glass-to-rubber transition of the amorphous part of the gelatin film and the second corresponding to the melting or dissociation of the ordered regions of the gelatin film. The glass transition temperature (ranging from 68 °C to 71 °C) and melting temperature (ranging from 102 °C to 107 °C) of the gelatin film was found to increase with an increase in solution drying temperature.[42,46,47] An average tensile strength of approximately 64 MPa, along with Young's modulus measuring around 2.5 GPa is estimated for the additive-free gelatin film by using tensile testing and is shown in Fig. S2 (ESI†). These mechanical properties are notably comparable to those of various other soft actuators. For instance, a soft actuator based on cellulose stearoyl esters possesses an elastic modulus of roughly 1.1 GPa.[48] Gelatin film with 50% PEDOT:PSS in solution shows an elastic modulus of about 3.4 GPa,[26] while a pollen paper-based soft actuator demonstrates maximum tensile strength and modulus values of about 40 MPa and 1.46 GPa, respectively.[31]

3.2. Vapor selective actuation of gelatin film

The bending and unbending behavior of the gelatin film upon exposure to and removal of water vapor is demonstrated in Movie S1 (ESI†). Snapshots of the film bending at different instances of water vapor exposure are shown in Fig. 2(a). To quantitatively analyze the actuation behavior, the gelatin film was fixed in a cantilever-like geometry, with one end clipped between two glass slides and the other free to move. Upon exposure to water vapor from the bottom side, the gelatin film rapidly bent upwards, achieving maximum curvature within ~1.4 seconds and maintaining this curvature as long as water vapor is present in the bottom side (Fig. 2(a)(i)–(iv)). Remarkably, when the water vapor source is withdrawn, the film quickly unbends and returns to its initial flat state (Fig. 2(a)(v) and (vi)). The entire experiment was conducted at a fixed environment temperature and humidity of 29 ± 1 °C and 50 ± 2%, respectively. The temporal evolution of the bending curvature of the film during water vapor exposure is displayed in Fig. 2(b). The actuation of the gelatin film in response to water vapor is rapid and fully reversible. The force generated by the gelatin film upon exposure to the water vapor is calculated by using the formula given below:[48]

$$F = \frac{E_s t^3 L k^2}{12(1-\nu^2)}, \quad (1)$$

where E_s is the elastic modulus, t is the thickness of the film, L is the length of the film, k is the bending curvature of the film, and ν is the Poisson's ratio. For the film with a length of 16 mm and thickness of 16 μm, the force is 182 μN. This force generated by the actuator is also the force exerted by the films on their surroundings. An experiment involving the actuation of the gelatin film upon exposure to water vapor under varying relative humidity conditions was conducted. The maximum bending curvature of the gelatin film at different relative humidity levels is shown in Fig. S3 (ESI†). To verify the repeatability of the actuation performance, the gelatin film was subjected to more than 1200 cycles of water vapor exposure while held in the cantilever-like geometry. Fig. 2(c) displays the bending curvature data for every 100th cycle of water vapor exposure. Notably, the bending curvature remained consistent after 1200 actuation cycles, confirming the stability in the actuation performance of the gelatin film. Small fluctuations in extremum curvature values can be attributed to localized humidity variations. The actuation characteristics of the gelatin film depend on its aspect ratio, thickness, and environmental conditions. We also investigate the effect of the water source temperature on the actuation characteristics of the gelatin film. A gelatin film of dimensions length = 20 mm, width = 10 mm, and thickness = 30 μm is fixed in a cantilever-like geometry. The bottom side of the film is exposed to water vapor coming from the water source maintained at three different temperatures (30 °C, 45 °C, and 55 °C). The snapshots of

Open Access Article. Published on 05 August 2024. Downloaded on 2/21/2026 9:32:34 AM.
This article is licensed under a Creative Commons Attribution-NonCommercial 3.0 Unported Licence.

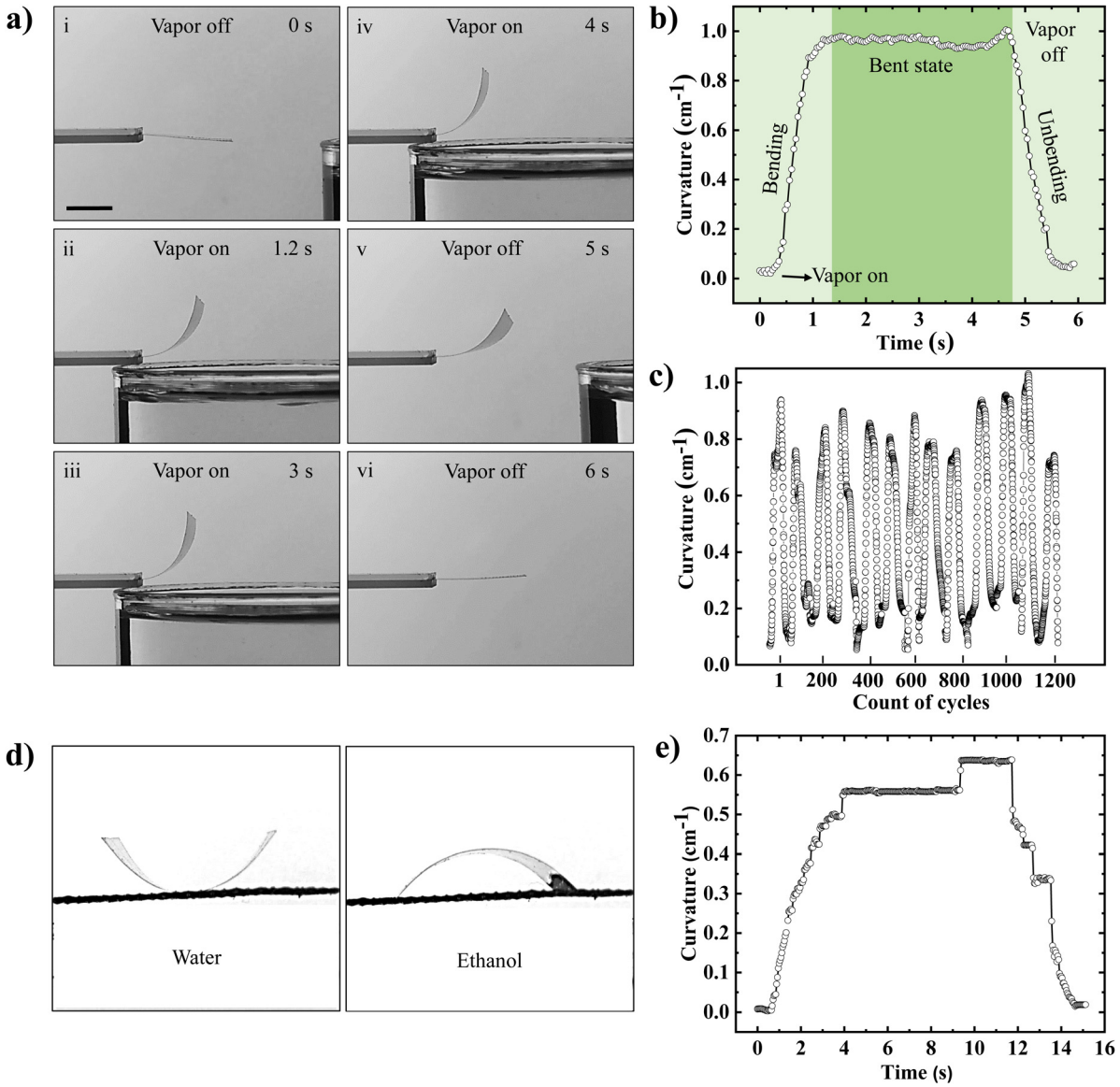

Fig. 2 (a) Snapshots extracted from the video recorded for a single cycle of bending and unbending of the gelatin film upon exposure to water vapor. (i) The flat state of the film in the absence of water vapor, (ii) the bent state after 1.2 s of water vapor exposure, (iii) and (iv) the maximum bending states. (v) and (vi) Returning pathway of the gelatin film upon withdrawal of the water vapor. Dimensions of the film: length, l = 16 mm, width, w = 15 mm, and thickness, t = 16 μm. The scale bar = 8 mm. (b) The temporal evolution of the bending curvature of the gelatin film upon exposure and removal of water vapor. (c) The bending curvature of the gelatin film for every 100th actuation cycle upon subjecting the film to 1200 continuous cycles of water vapor exposure. Dimensions of the film: l = 17 mm, w = 15 mm, t = 18 μm. (d) The images on the left and right sides depict the upward and downward bending of the gelatin film upon exposure to the water and ethanol vapor, respectively. (e) The temporal evolution of the bending curvature of gelatin film upon exposure and removal of ethanol vapor. The dimensions of the film: l = 34 mm, w = 25 mm, t = 18 μm.

the maximum bending state of the film are shown in Fig. S4(a) (ESI†). The time evolution of bending curvature upon exposure to the water vapor coming from the source maintained at three different temperatures is shown in Fig. S4(b) (ESI†). We note that the temperature of the water source plays a major role in the actuation characteristics of the gelatin film. The bending curvature of the film is minimum at 30 °C source temperature and maximum at 55 °C source temperature. We also calculated the actuation pace for all three vapor source temperatures, which is minimum (0.2081 cm^{-1} s^{-1}) for 30 °C and maximum (0.6618 cm^{-1} s^{-1}) for 55 °C source temperature. The increase in the water source temperature leads to higher saturation water vapor pressure, and more water molecules can be accommodated in the air so that the actuator can absorb more water molecules and achieve higher deformation. Aside from its rapid, reversible, and repeatable actuation response to water vapor, the gelatin film also demonstrates a unique response to ethanol vapor. The gelatin film exhibits an upward bending upon exposure to water vapor, while the film shows a downward bending upon exposure to ethanol vapor, as shown in Fig. 2(d). As can be inferred from the right panel of Fig. 2(d), a gelatin film with dimensions l = 34 mm, w = 25 mm, and t = 18 ± 1 μm kept on a mesh bends

© 2024 The Author(s). Published by the Royal Society of Chemistry

Open Access Article. Published on 05 August 2024. Downloaded on 2/21/2026 9:32:34 AM.
This article is licensed under a Creative Commons Attribution-NonCommercial 3.0 Unported Licence.

downward upon exposure to ethanol vapor from the bottom side. The gelatin film reaches its maximum curvature of approximately 0.65 cm^{-1}, under a continuous supply of ethanol vapor. Notably, the gelatin film returns to its initial state after the removal of the vapor source from beneath the film. This establishes the fast and fully reversible actuation characteristics of gelatin actuators upon ethanol vapor exposure. The temporal evolution of the bending curvature of the gelatin film in response to ethanol vapor exposure is shown in Fig. 2(e). The time evolution of the bending curvature of gelatin film upon exposure to other solvent vapors, such as heptanol, pentanol, butanol, and ethanol, is measured and shown in Fig. S5(a) (ESI†). Remarkably, the bending curvature of the gelatin film changes in accordance with the polarity of the solvents upon exposure to different solvent vapors. The polarity of the solvents exhibits an increasing trend from heptanol (0.549) to ethanol (0.654). Additionally, the curvature aligns with this ascending order, ranging from 0.15 cm^{-1} for heptanol to 0.65 cm^{-1} for ethanol. The maximum bending curvature value of the gelatin film as a function of the vapor pressure of the respective solvents is shown in Fig. S5(b) (ESI†).

3.3. Actuation mechanism

Gelatin, derived from collagen found in animal connective tissues, is composed of several amino acids containing hydrophilic groups, such as amino and carboxyl groups, as depicted in the upper panel of Fig. S6 (ESI†).[33,34] As a result of the presence of these functional groups, gelatin displays a hydrophilic characteristic. On the left side of Fig. 3(a), a gelatin film is fixed in a cantilever-like configuration and remains in its initial flat state in the absence of water vapor on the bottom side.

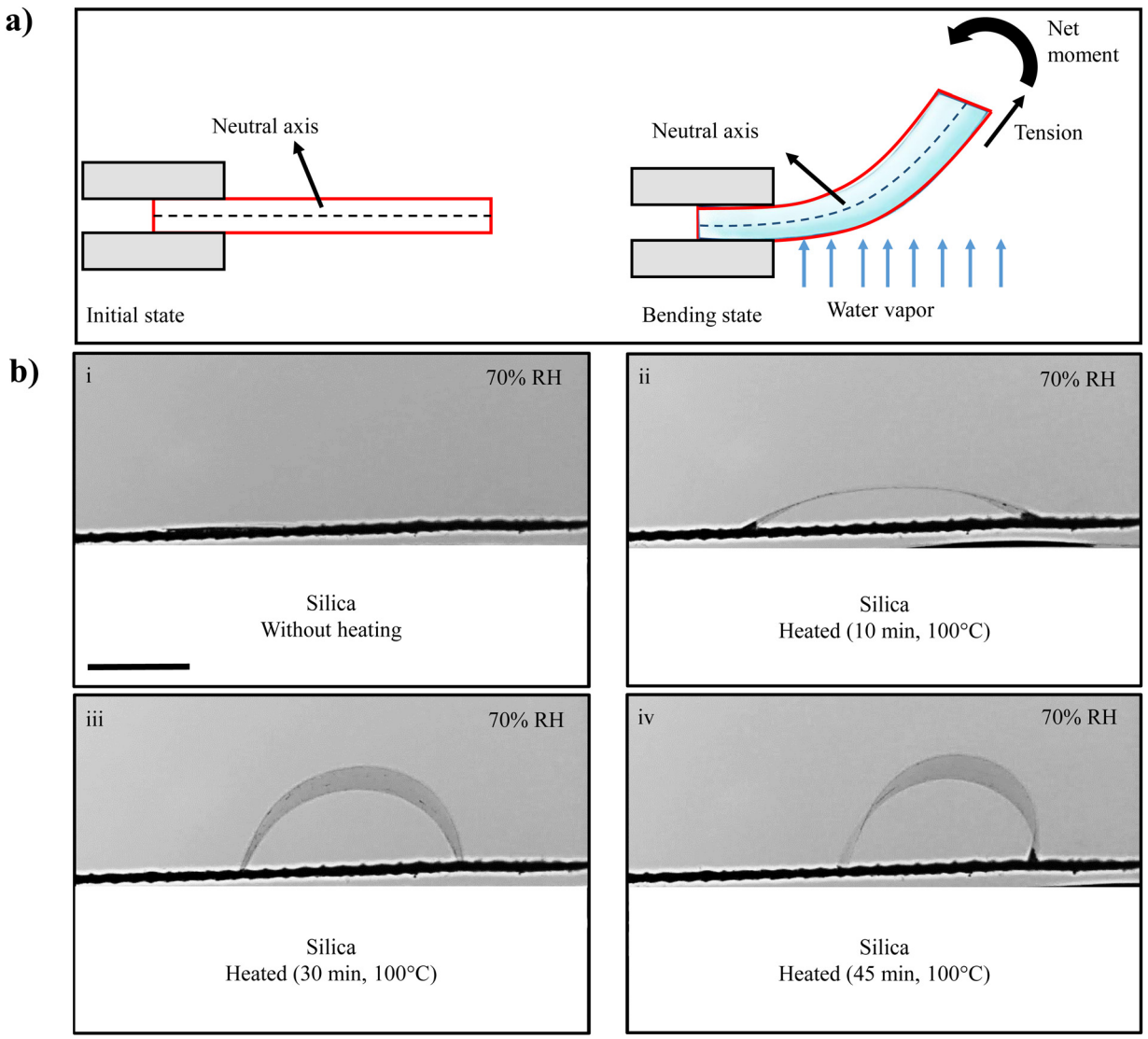

Fig. 3 (a) Illustrates the bending mechanism of the gelatin film upon exposure to the water vapor from beneath. On the left side, the gelatin film is in its initial flat state in the absence of water vapor. The right side shows the bending state of the gelatin film in the presence of water vapor on the bottom side. (b) (i)–(iv) Show the snapshots of gelatin film bending upon exposure to silica gel (dehydrated at 100 °C for different times) at fixed atmospheric relative humidity 70%. Dimensions of the film: l = 30 mm, w = 25 mm, and t = 30± 1 μm. The scale bar = 10 mm.

Open Access Article. Published on 05 August 2024. Downloaded on 2/21/2026 9:32:34 AM. This article is licensed under a Creative Commons Attribution-NonCommercial 3.0 Unported Licence.

However, upon exposure to water vapor from the bottom side, the hydrophilic groups within the gelatin film react with water molecules *via* hydrogen bonds, leading to the absorption of water vapor, as illustrated in the lower panel of Fig. S6 (ESI†). As a consequence of water absorption by the gelatin film, its lower surface swells due to the higher humidity in comparison to the upper surface. This phenomenon gives rise to the development of tensile strain and progressively diminishes from the bottom surface towards the top surface, resulting in a strain gradient along the thickness of the gelatin film. This vertical strain gradient, in turn, generates a vertical stress gradient within the film, leading to a net bending in the upward direction. Consequently, the film bends upward, as demonstrated on the right side of Fig. 3(a). This mechanism, where bending occurs due to a swelling-induced vertical stress gradient within the film upon exposure to vapors, has also been elucidated by other researchers.[16,49,50] To validate the water absorption capability of the gelatin film, a swelling experiment using liquid water was conducted. A square-shaped gelatin film measuring 16 mm in dimension was immersed in liquid water, and images were captured before and after 30 seconds of immersion in water, as depicted in Fig. S7 (ESI†). Within this brief 30-second time interval, the gelatin film underwent a noticeable transformation, with its length and width expanding from 16 to 28 mm, clearly demonstrating the substantial water absorption capacity of the gelatin film. However, the distinct downward bending of the gelatin film when exposed to ethanol vapor suggests that the mechanism is different from the swelling-induced stress gradient observed in water vapor. Something else drives the gelatin film to curve in the opposite direction when exposed to ethanol vapor.

The upward bending of the gelatin film results from swelling brought about by the absorption of water molecules on the lower side of the film. Conversely, the downward bending can be attributed to contraction, which occurs due to the desorption of water molecules from the lower side when exposed to ethanol vapor. This desorption process is likely prompted by the presence of ethanol vapor, which has a desiccating effect on the lower surface of the film. We note a similar observation by Gu Yuanqing *et al.*,[51] where they studied the behavior of polyethyleneimine/poly(acrylic acid) multilayer films when exposed to polar organic solvents. In their research, they observed that these films underwent contraction due to the removal of water molecules when exposed to organic solvents. Fig. 2(a) in their study[51] clearly illustrates the swelling of the film in DI water and its shrinkage in ethanol, providing visual evidence of this phenomenon. Their research revealed that exposure to organic solvents generated a localized water activity gradient within the film and its surroundings, leading to water extraction. This finding supports the observed desorption-induced contraction in similar materials. Furthermore, G. Manikandan *et al.*[19] have also reported similar downward bending behavior in silk films, which occurs due to the desiccation of water molecules in the presence of ethanol vapor. This consistent behavior across different materials underscores the role of water desorption in inducing downward bending when exposed to certain organic solvent vapors. To investigate this hypothesis, a gelatin film was subjected to dehydrated silica gel (well-known for its water-removal capabilities) from beneath. Dehydrated silica gel is commonly employed in industrial packaging to safeguard items from humidity-related damage. In the experimental setup, a gelatin film with both ends free was placed on a mesh, with atmospheric humidity maintained at 70%, and exposed to dehydrated silica gel heated to 100 °C for different time durations (0, 10, 30, and 45 minutes). As expected, when exposed to hydrated silica gel, the gelatin film remained flat and did not exhibit any bending (Fig. 3(b)(i)). In contrast, exposure to dehydrated silica gel from beneath induced downward bending in the gelatin film, as depicted in Fig. 3(b)(ii)–(iv). Notably, the gelatin film promptly reverted to its original flat state upon removal of the silica gel. As the heating time of silica gel increased, the maximum downward bending curvature of the gelatin film also increased, as illustrated in Fig. 3(b)(ii)–(iv). This effect was quantitatively confirmed by measuring the bending curvature of the gelatin film upon exposure to silica gel dehydrated for different durations, as shown in Fig. S8 (ESI†). As a result, the downward curvature can be attributed to the contraction of the lower surface of the film caused by the release of water molecules. The similarities observed in the response of the gelatin film to ethanol and dehydrated silica gel strongly imply that the presence of ethanol vapor indeed triggers a desiccation effect within the gelatin film. To further confirm this, we continuously monitored the weight of the gelatin film in an ethanol vapor environment and plotted it over time, as illustrated in Fig. S9 (ESI†). It is worth noting that the weight of the gelatin film decreases in the presence of ethanol vapor, providing clear evidence of the desiccation of water molecules from the gelatin film.

3.4. Effect of salt and sugar on the actuation

The addition of salt and sugar has been shown to significantly alter the physical properties of the gelatin film, as reported previously.[52,53] Examining how sugar and salt affect the actuation behavior of the gelatin film is of scientific interest. To elucidate this phenomenon, a gelatin film with varying salt concentrations (0%, 2.5%, and 5% relative to the gelatin content) is firmly clamped between two glass slides arranged in a cantilever-like configuration. Subsequently, the film is exposed to water vapor from the bottom side. Owing to the absorption of water vapor, the film exhibited an upward bending, ultimately returning to its original state upon removing the water vapor. Notably, our observations revealed that introducing salt into the gelatin solution considerably increased the bending curvature of the gelatin film, as depicted in Fig. 4(a). As reported previously, adding salt to the gelatin weakens the intermolecular forces between the chains, thus increasing the free volume and swelling of the gelatin film significantly.[52] Consequently, the heightened swelling capability and the augmented free volume culminate in the amplified bending curvature of the gelatin film upon exposure to water vapor.

Similarly, a progressive augmentation in the bending curvature of the gelatin film was observed upon the addition of sugar at varying concentrations (0%, 5%, and 10% relative to the gelatin content),

 © 2024 The Author(s). Published by the Royal Society of Chemistry

Open Access Article. Published on 05 August 2024. Downloaded on 2/21/2026 9:32:34 AM.
This article is licensed under a Creative Commons Attribution-NonCommercial 3.0 Unported Licence.

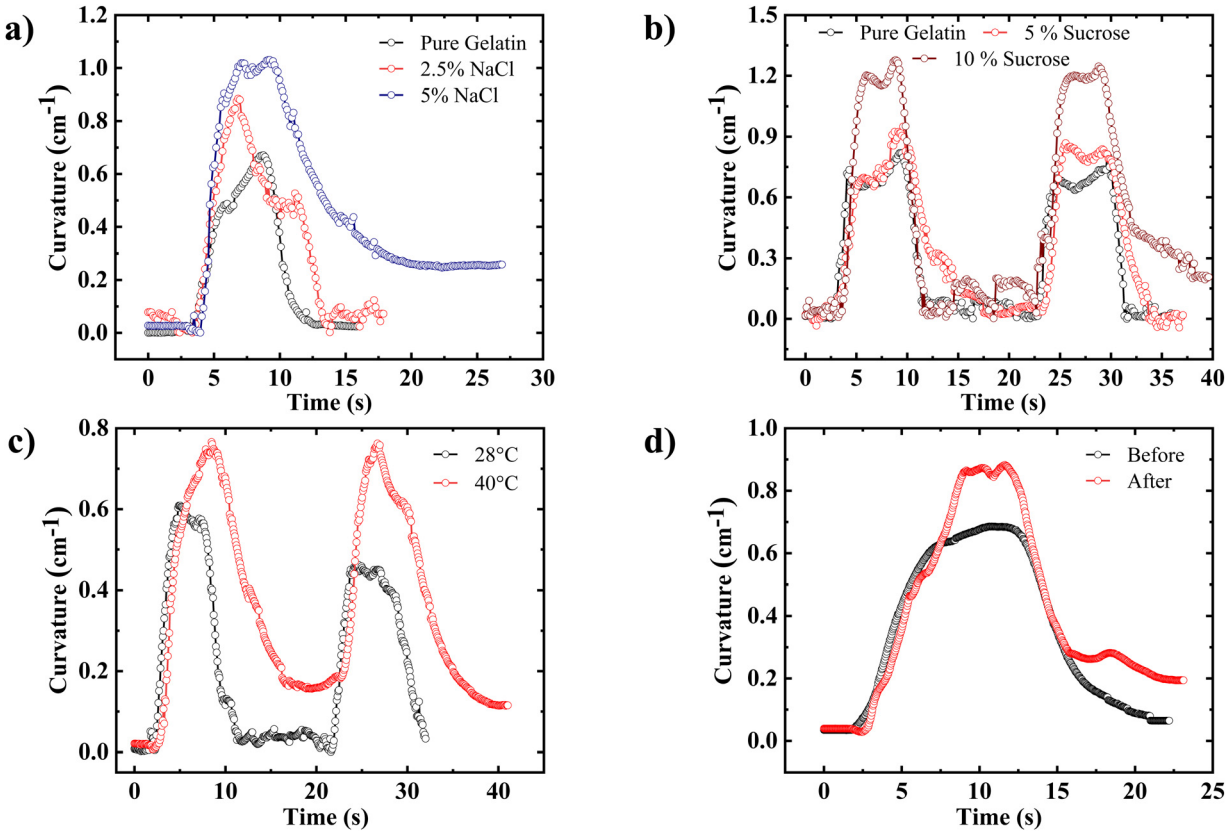

Fig. 4 (a) and (b) The temporal evolution of the bending curvature of the gelatin film by the addition of salt and sugar upon exposure to water vapor, respectively. Dimension of the film (salt): l = 13 mm, w = 10 mm and t = 21 μm. Dimensions of the film (sugar): l = 13 mm, w = 10 mm and t = 14 μm. (c) The temporal evolution of the bending curvature of the gelatin films prepared by solutions dried at 28 °C (black) and 40 °C (red). Dimensions of the film: l = 15 mm, w = 12 mm, and t = 26 ± 1 μm. (d) The temporal evolution of the bending curvature of the gelatin film before and after annealing at 50 °C for 1 hour in a hot air oven. Dimensions of the film: l = 25 mm, w = 20 mm, and t = 30 μm.

as depicted in Fig. 4(b). Introducing sugar into the gelatin matrix instigates notable alterations in its molecular dynamics. Specifically, it reduces intermolecular pressure, enhancing polymer chain mobility, flexibility, and extensibility, as reported in a recent article.[54] Additionally, incorporating sugar into the gelatin matrix augments its water absorption capacity, facilitating the establishment of a robust network for water retention within the gelatin film, in agreement with previous investigations.[53] Consequently, this increased water absorption capacity, coupled with enhanced polymer chain mobility and extensibility, collectively contribute to the propensity of the gelatin film to exhibit larger bending curvature when exposed to water vapor.

3.5. Effect of drying temperature on the actuation

The molecular structure of the gelatin film undergoes changes depending on the drying conditions of the gelatin solution.[42] Therefore, it is intriguing to explore how the structure of the gelatin film affects its actuation behavior. To investigate this, a 3 wt% gelatin solution was poured into a petri dish and dried at two different temperatures: 28 ± 1 °C and 40 ± 1 °C, in a constant 60% RH. To study the effect of drying temperature on the molecular structure of the gelatin film, X-ray diffraction patterns were recorded for the gelatin films dried at 28 ± 1 °C and 40 ± 1 °C (see Fig. S10, ESI†). It was observed that as the drying temperature increased from 28 ± 1 °C to 40 ± 1 °C, the amount of triple helix in the gelatin film decreased, evident from the decrease in peak intensity at $2\theta = 7^{\circ}$, which corresponds to the triple helix content in the film. This observation is consistent with previous reports.[42,46] To investigate actuation behavior, gelatin films in a cantilever-like configuration were exposed to water vapor from the bottom side. We note that increasing the solution drying temperature led to a corresponding increase in the bending curvature of the gelatin film, as demonstrated in Fig. 4(c) and Movie S2 (ESI†). However, it's worth noting that the unbending process was slower than the initial bending, and full reversibility wasn't achieved for the film dried at 40 ± 1 °C, possibly due to incomplete water desorption from the gelatin film. The increased bending curvature in this film can be attributed to its higher water absorption capacity. As the solution drying temperature increases, the ordered content of gelatin film diminishes while its coil structure expands. This coiled gelatin exhibits greater water absorption capacity at high relative humidity levels, explaining the higher bending curvature observed in the film dried at 40 ± 1 °C.[42,55]

3.6. Effect of the post-annealing on the actuation

The impact of post-fabrication annealing by increasing the temperature on the actuation behavior of gelatin was studied.

Open Access Article. Published on 05 August 2024. Downloaded on 2/21/2026 9:32:34 AM.
This article is licensed under a Creative Commons Attribution-NonCommercial 3.0 Unported Licence.

To accomplish this, the actuation response of the gelatin film to water vapor exposure was recorded both before and after subjecting the film to annealing at 50 °C for 1 hour. The temporal evolution of the bending curvature of the gelatin film before and after annealing is shown in Fig. 4(d). Interestingly, it was observed that the bending curvature of the gelatin film increased after undergoing the annealing process. However, despite this enhancement in curvature, the film did not fully return to its initial flat state upon the removal of water vapor, as demonstrated in Movie S3 (ESI†). Previously, it has been reported that bound water molecules are present in the helical structure of gelatin or collagen, and they play a pivotal role in stabilizing the triple helix structure by forming inter-chain hydrogen bonding.[56,57] However, during annealing, these bound water molecules are released, leading to a less stable structure that tends to adopt coil formations. Consequently, it is speculated that after annealing, the gelatin film can accommodate more water by filling the vacant bound water sites with free water, resulting in an increased bending response of the gelatin film to water vapor exposure. Nonetheless, due to a relatively lower amount of water desorption or solely free water desorption, the film does not fully return to its initial state after removing water vapor (see Fig. 4(d)).

3.7. Control over the actuation: magnitude and direction

The gelatin film displayed distinct bending responses upon exposure to water and ethanol vapors, offering a unique avenue for controlling its actuation performance and maximum curvature. Intriguing actuation characteristics can be harnessed by exposing the gelatin film to vapors generated from binary solutions with varying water-to-ethanol ratios (W : E = 100 : 0, 80 : 20, 40 : 60, 20 : 80, 10 : 90, 0 : 100).

To demonstrate this phenomenon, a gelatin film was placed on a wire mesh and exposed to vapor emanating from a binary

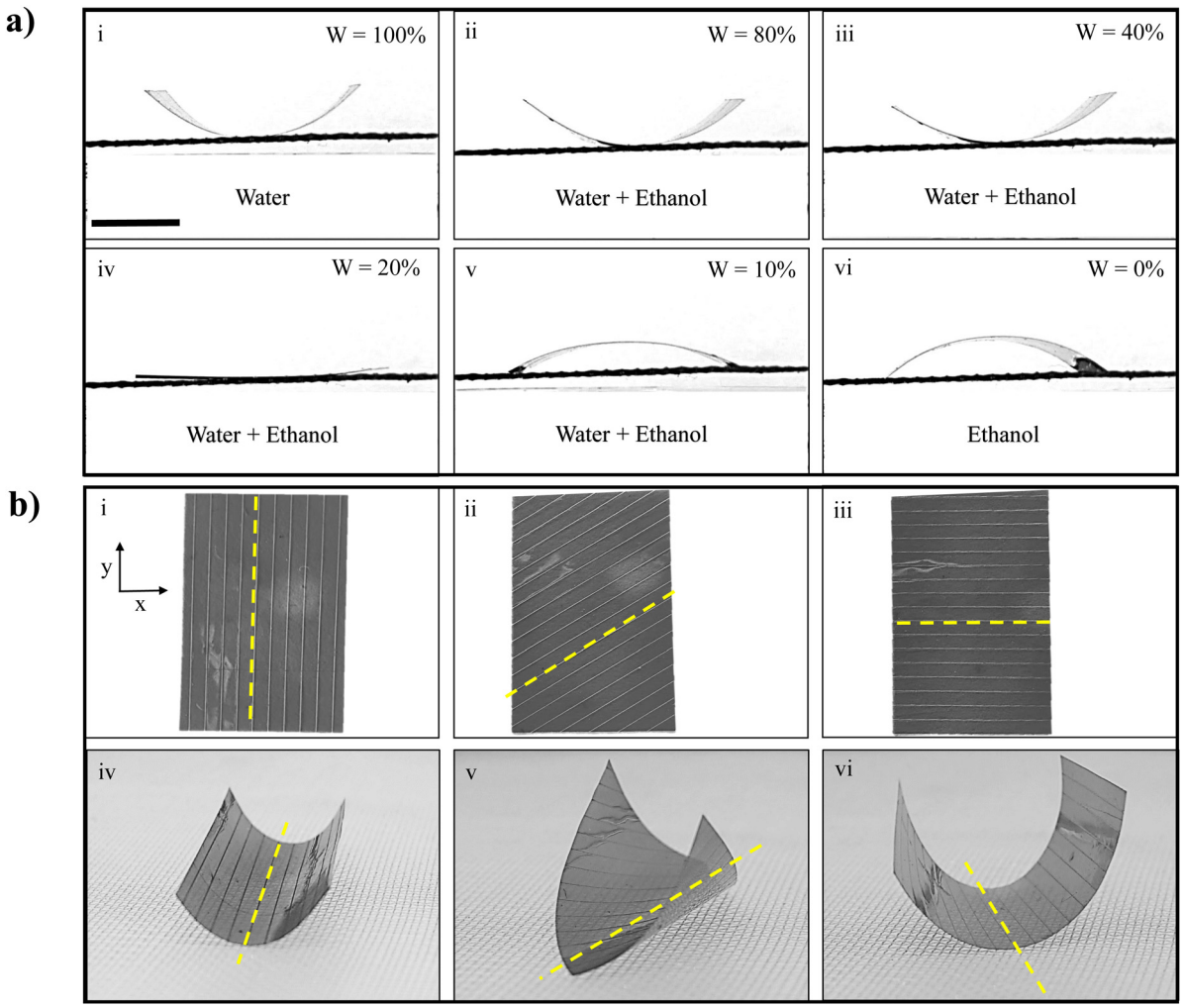

Fig. 5 (a) Snapshots displaying the maximum bending curvature attained when exposing the films to the vapor emitted from a binary water and ethanol solution at various ratios for a duration of 3 seconds. Dimensions of the film: l = 30 mm, w = 25 mm, and t = 30 ± 1 μm. The scale bar = 10 mm. (b) Patterning of the surface provides a way to control the bending axis: (i) the pattern is oriented parallel, (ii) at 45°, and (iii) perpendicular to the y-axis (marked by a yellow dashed line). (iv)–(vi) Depict the corresponding bending state of patterned gelatin films upon exposure to water vapor from the bottom side (the yellow dashed line marks the bending axis).

© 2024 The Author(s). Published by the Royal Society of Chemistry

Open Access Article. Published on 05 August 2024. Downloaded on 2/21/2026 9:32:34 AM. This article is licensed under a Creative Commons Attribution-NonCommercial 3.0 Unported Licence.

solution composed of water and ethanol in various ratios. Snapshots capturing the bending state of the gelatin film after a 3 seconds exposure to these vapor mixtures are shown in Fig. 5(a). As the ethanol concentration in the binary solution increased, the upward bending curvature progressively decreased, eventually ceasing entirely at a water-to-ethanol ratio of 20 : 80 in the binary solution, as illustrated in Fig. 5(a)(iv). Moreover, as the ethanol concentration continued to increase in the binary solution, the gelatin film exhibited a reversal in its bending direction, now bending downward, as observed in Fig. 5(a)(v) and (vi). The role of partial pressures on the degree of actuation due to vapors generated from a mixture of water and ethanol vapors has been calculated using Raoult's law[58] and shown in Table S1 (ESI†). It can be observed that with the increase in ethanol in liquid water, the partial pressure of water decreases. As expected, the direction of the bending of the film also changes accordingly. In addition to controlling the magnitude of actuation, precise manipulation of the bending axis in the actuation direction holds significant importance in various contemporary soft actuator applications. To achieve this control, we engineered gelatin films with specific periodic patterns (the details of which are outlined in the Methodology section). These patterns are oriented at angles of 0°, 45°, and 90° relative to the *y*-axis, as illustrated in Fig. 5(b)(i)–(iii). Remarkably, upon exposure to water vapor, it was observed that the bending axis of the patterned gelatin film is always parallel to the pattern orientations, as shown in Movie S4 (ESI†) and corresponding snapshots in Fig. 5(b)(iv)–(vi). This observation implies that the bending energy of the gelatin film is reduced along the direction of the patterns, enabling the film to bend in a specific direction determined by the pattern orientation. This precise control over the actuation direction enhances the versatility and potential of gelatin-based soft actuators for a wide range of applications. Moreover, the surface patterning of the film serves a dual purpose: it not only provides precise control over the bending axis but also significantly enhances the maximum bending curvature of the film. To demonstrate this effect, gelatin films (with smooth and patterned surfaces) with dimensions l = 15 mm, w = 13 mm, and t = 25 ± 1 μm were clamped between two glass slides in a cantilever-like configuration. Subsequently, the films were exposed to water vapor from the bottom side, and actuation was recorded as shown in Movie S5 (ESI†). The quantitatively measured time evolution of bending curvature is shown in Fig. S11 (ESI†). Notably, the patterned film exhibited a bending curvature that was 95% higher than the smooth film.

3.8. Random locomotion to linear motion

The phenomenon of locomotion of the gelatin film in response to water vapor holds significant promise with many applications in materials science and biomimetics. To probe the locomotion properties, a 4 cm diameter gelatin film was placed on a plastic mesh and exposed to water vapor from the bottom side.

The gelatin film, owing to its inherent hygroscopic nature, rapidly absorbed moisture from the vapor source, leading to an upward bending deformation. This bending arose from differential moisture absorption across the thickness of the film, resulting in a shift in the center of gravity of the film and generating a mechanically unstable state. Consequently, the gelatin film tilted and toppled onto a side where it distanced itself from the water vapor source. In this new orientation, the film initiated moisture loss from the surface facing away from the vapor, leading to flattening while simultaneously absorbing water on the exposed surface. It is worth noting that the direction of the next flipping cycle remained unpredictable. This cyclic interplay of water absorption and desorption within the gelatin film created a rhythmic locomotion pattern, driven by the water vapor exposure, as displayed in Fig. 6(a)

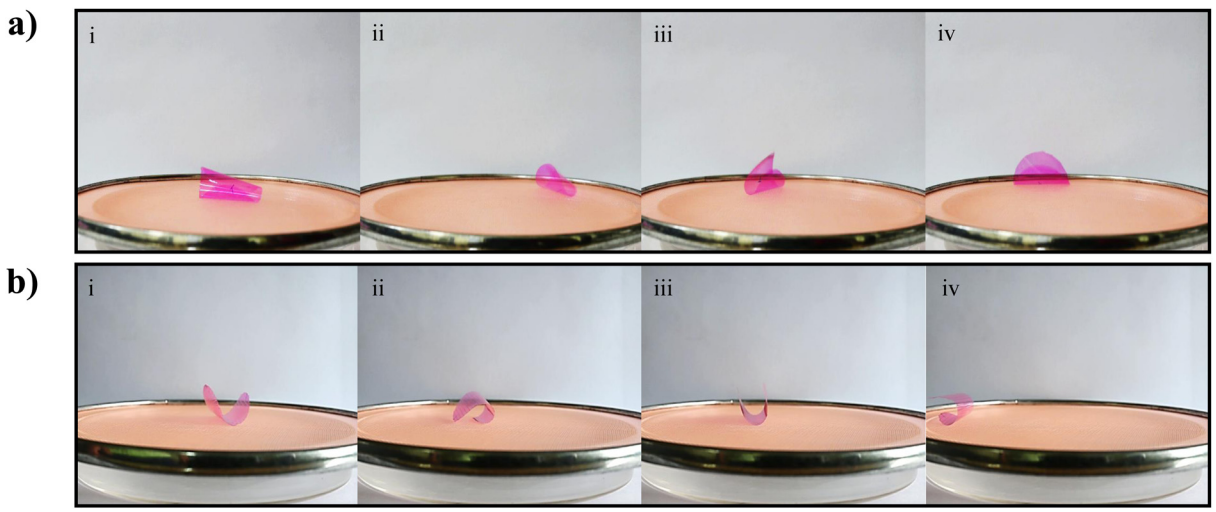

Fig. 6 (a) Snapshots of the circular-shaped non-patterned gelatin film at different times while doing locomotion upon exposure to water vapor from the bottom side. The dimensions of the film: diameter = 4 cm and thickness = 15 ± 3 μm. (b) Snapshots of the circular-shaped patterned gelatin film at different times while undergoing a linear motion upon exposure to water vapor from the bottom side. The dimensions of the film: diameter = 4 cm and t = 20 ± 3 μm.

Open Access Article. Published on 05 August 2024. Downloaded on 2/21/2026 9:32:34 AM. This article is licensed under a Creative Commons Attribution-NonCommercial 3.0 Unported Licence.

and Movie S6 (ESI†). To harness this gelatin film locomotion and convert it into controlled linear motion, we introduced a periodic surface pattern on the gelatin film having a 4 cm diameter. Placing such a patterned film on a plastic mesh exposes water vapor from the bottom side, leading to an anticipated upward bending of the film and subsequent flipping. Notably, the presence of the periodic surface pattern played a crucial role in directing the ensuing locomotion dynamics. The presence of the patterns constrained bending behavior in specific directions, guiding the subsequent flipping actions in a controlled manner along one direction, as displayed in Fig. 6(b) and Movie S6 (ESI†). This innovative approach effectively transformed the random locomotion of the gelatin film into purposeful linear motion, offering promising applications in responsive materials and bioinspired actuation systems. Similarly, the transformation of locomotion into linear motion in a square-shaped gelatin film was achieved by patterning its surface, as depicted in Fig. S12(a and b) and Movie S7 (ESI†). Finally, the actuation performance of the gelatin-based vapor-responsive soft actuators without any additives, presented in this study, has been compared with other gelatin and non-gelatin-based soft actuators, displayed in Table S2 in the ESI.† It is germane to note that the durability and retention of actuation performance without any noticeable fatigue over 1200 actuation cycles, multi-vapor responsiveness leading to control of the actuation magnitude and direction, and exploiting surface patterns to enhance functionality further are unique features presented in this work.

4. Applications

In this section, we demonstrate a few proof-of-concept applications of the additive-free gelatin film-based biocompatible soft actuators by exploiting their vapor-responsive actuation behavior. A gelatin-based soft actuator can be a key component in developing robotic systems capable of sensing ethanol and other toxic vapors. To demonstrate, a rectangular-shaped gelatin film was placed on the plastic mesh, and a thin aluminum strip was pasted on the middle of the film to impart electrical conductivity (Fig. 7(a)).

This conducting gelatin-based actuator is integrated into an electrical circuit connected with an LED through a battery. Initially, the circuit is open, and the LED is off in the absence of ethanol vapor under the gelatin film, as shown in the upper panel of Fig. 7(a). As soon as ethanol vapor was released from the bottom side, the gelatin film started to bend and close the circuit by connecting two hanging electrodes, resulting in an

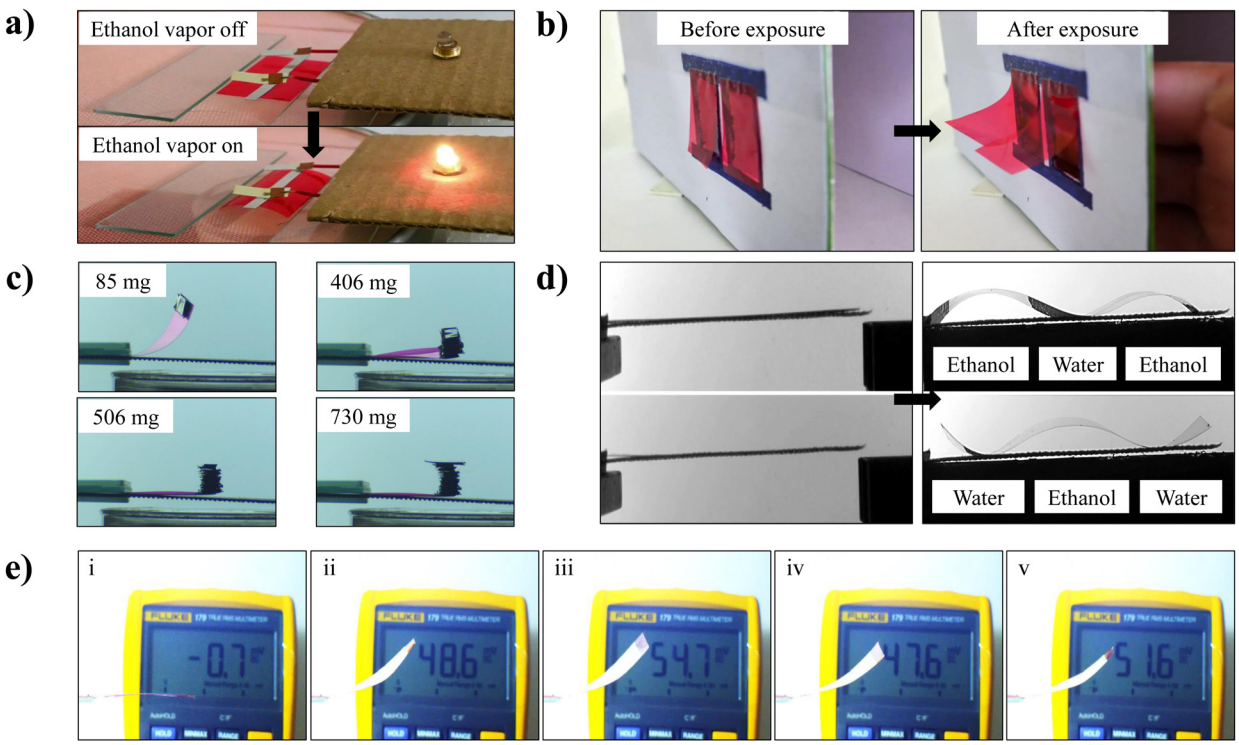

Fig. 7 (a) Gelatin film as an ethanol vapor sensor: in the upper panel, the film is in a flat state in the absence of ethanol. In the lower panel, the gelatin film bends downward in the presence of ethanol vapor and closes the electric circuit, resulting in an LED glow. (b) Humidity-gated smart curtains: in the left panel, curtains are closed in the absence of the stimulus. In the right panel, the curtain opens when a bare human hand is in close proximity. (c) Smart lift: the weight lifting capacity of the gelatin film. It can lift the weight up to several milligrams upon exposure to water vapor. (d) Wave motion of the gelatin film in a programmed stimulus of water and ethanol vapors. In the upper panel, the film makes an ''M'' shape upon exposure to the vapor sequence ethanol–water–ethanol. In the down panel, the film makes a ''W'' shape when the vapor sequence is water–ethanol–water. (e) Snapshots corresponding to the voltage generation by the gelatin–PVDF assembly under exposure to water vapor from the bottom side for multiple cycles.

© 2024 The Author(s). Published by the Royal Society of Chemistry

Open Access Article. Published on 05 August 2024. Downloaded on 2/21/2026 9:32:34 AM. This article is licensed under a Creative Commons Attribution-NonCommercial 3.0 Unported Licence.

LED glow as shown in Movie S8 (ESI†) and the bottom panel of Fig. 7(a). When the ethanol vapor is cut off, the film returns to its initial position, resulting in an off-state for the LED. Integration of these actuators into the robotic devices deployed in industrial settings in the presence of organic solvent vapors may be useful in environmental monitoring, industrial automation, and safety inspection. Next, the use of a gelatin-based actuator for the manipulation and control of humidity-gated smart curtains is demonstrated. A rectangular-shaped gelatin film was pasted on the opening in the enclosed box as shown in the left panel of Fig. 7(b). As a bare human palm approaches the curtain from inside, the curtain opens as shown on the right side of Fig. 7(b), and closes back after the extraction of the human palm as can be seen in Movie S9 (ESI†). These smart curtains can be useful in remote-sensing windows due to their low cost and ease of fabrication. Furthermore, a smart lift based on the gelatin film is fabricated, where it uses a small amount of water vapor and converts it into mechanical work by lifting the attached weight in a controlled manner. A few milligrams of weight are attached at one end of the gelatin film, and the other end is clamped. Upon exposure to the water vapor from the bottom side, the film bends upward with attached weight, as shown in Movie S10 (ESI†) and in Fig. 7(c). As can be observed from the figure, the maximum attainable height of the film decreases with an increase in the mass of the attached cargo. The magnitude of the lifting force generated by the film upon exposure to the water vapor is estimated by the formula $F = mg$, where m is the mass attached to the film and g is the acceleration of gravity. The upward bending is found to be negligibly small for an attached mass of 720 mg. The lifting force generated by the film is estimated to be about approximately 7.2 mN. It is noted that this lifting force is strongly related to the geometrical shape of the actuator. Moreover, these additive-free gelatin films can lift about 25 times their own weight in response to ethanol vapor, as shown in Fig. S13 (ESI†). The multi-vapor responsive nature of the gelatin film can be explored to generate complex shapes. The gelatin-based soft actuator has the capability to generate undulated wave motion or worm-like motion through simple sequential exposure to different vapors, which opens up exciting possibilities for the development of advanced soft robotic systems with enhanced functionality and versatility. To demonstrate, a gelatin film was kept on the wired mesh and exposed to water and ethanol containers attached sequentially. Due to the distinct behavior of the gelatin film in water and ethanol vapors, the film bends downwards at both ends and upward in the middle, as shown in the upper panel of Fig. 7(d) and *vice versa* upon interchanging the position of water and ethanol as shown in the lower panel in Fig. 7(d) (Movie S11, ESI†). Lastly, the vapor-responsive properties of gelatin films are exploited to generate electrical voltage when exposed to water vapor. To achieve this, a piezoelectric silver electrode-coated polyvinylidene fluoride (PVDF) film, with dimensions length = 35 mm, width = 25 mm, and thickness = 28 μm was attached to the gelatin film. The top and bottom electrodes of the PVDF film are connected to a multimeter. This assembly was fixed in a cantilever-like configuration, with the PVDF film on top of the gelatin film, as shown in Fig. 7(e)(i). When the gelatin film was exposed to water vapor from the bottom side, it bent upward, causing bending in the attached piezoelectric PVDF film. This bending led to the generation of electrical voltage, leveraging the piezoelectric nature of the PVDF film. This basic system is capable of producing electrical voltage, ranging from 47 to 54 mV, as displayed in Movie S12 (ESI†) and Fig. 7(e)(ii)–(v).

5. Conclusions

In summary, our study reveals the remarkable capabilities of a fully biodegradable and biocompatible vapor-responsive soft actuator constructed from gelatin without any additives. This exceptional actuator exhibits rapid, completely reversible, and vapor-selective actuation properties. Utilizing a cost-effective solution casting technique, we engineered gelatin-based actuators that exhibit distinct bending responses to different stimuli vapors. They exhibit an upward bending when exposed to water vapor and a downward bending motion when exposed to ethanol vapor. By adjusting the water and ethanol ratios in a binary solution, we achieved precise control over the magnitude of actuation, even capable of completely suppressing it at specific solvent ratios. The gelatin film demonstrated remarkable stability and repeatability, enduring more than 1200 continuous actuation cycles without any noticeable performance degradation. The impact of adding salt and sugar, drying temperature, and post-annealing on actuation performance are also investigated. Moreover, the incorporation of periodic patterns on the surface of the gelatin not only allowed us to control the bending axis but also significantly enhanced the actuation performance of the gelatin-based actuator. This surface patterning also transformed random locomotion into linear motion of the gelatin film in response to water vapor. The ability of the actuator to selectively respond to different vapor stimuli opens up exciting possibilities for a wide range of applications, including ethanol vapor detection, weightlifting, humidity-regulated smart curtains, wave-like motion generation, and voltage generation. These findings pave the way for the seamless integration of gelatin-based soft actuators into the rapidly evolving field of soft robotics and offer precision in controlling both the magnitude and direction of actuation.

Author contributions

Vipin Kumar: conceptualization, data curation, formal analysis methodology, validation, visualization, writing – original draft. Sarah Ahmad Siraj: data curation, writing – review & editing. Dillip K. Satapathy: conceptualization, methodology, funding acquisition, investigation, resources, supervision, writing – review & editing.

Data availability

The data supporting this article have been included as part of the ESI.†

Open Access Article. Published on 05 August 2024. Downloaded on 2/21/2026 9:32:34 AM. This article is licensed under a Creative Commons Attribution-NonCommercial 3.0 Unported Licence.

Conflicts of interest

There are no conflicts to declare.

Acknowledgements

The authors acknowledge financial support from the Ministry of Education, Government of India, through the Scheme for Transformational and Advanced Research in Sciences (STARS) and the generous financial support from IIT Madras under the Institutes of Eminence (IoE) scheme funded by the Ministry of Education, Government of India.

References

1 A. G. Volkov, J. C. Foster, T. A. Ashby, R. K. Walker, J. A. Johnson and V. S. Markin, *Plant, Cell Environ.*, 2010, **33**, 163–173.
2 H. Quan, A. Pirosa, W. Yang, R. O. Ritchie and M. A. Meyers, *Acta Biomater.*, 2021, **128**, 370–383.
3 S. Tang, Z. Davoudi, G. Wang, Z. Xu, T. Rehman, A. Prominski, B. Tian, K. M. Bratlie, H. Peng and Q. Wang, *Chem. Soc. Rev.*, 2021, **50**, 12679–12701.
4 A. Khan, K. A. Alamry and R. K. Jain, *RSC Adv.*, 2019, **9**, 39721–39734.
5 W. Ma, D. Hua, R. Xiong and C. Huang, *Mater. Adv.*, 2023, **4**, 458–475.
6 J. Wei, S. Jia, J. Wei, C. Ma and Z. Shao, *ACS Appl. Mater. Interfaces*, 2021, **13**, 38700–38711.
7 Q. Wang, Z. Wu, J. Li, J. Wei, J. Guo and M. Yin, *ACS Appl. Mater. Interfaces*, 2022, **14**, 38972–38980.
8 Y. Wang, Q. Guo, G. Su, J. Cao, J. Liu and X. Zhang, *Adv. Funct. Mater.*, 2019, **29**, 1906198.
9 V. Kumar, S. A. Siraj and D. K. Satapathy, *ACS Appl. Mater. Interfaces*, 2024, **16**, 3966–3977.
10 D. Zhalmuratova and H.-J. Chung, *ACS Appl. Polym. Mater.*, 2020, **2**, 1073–1091.
11 T. Brossier, M. Habib, B. T. Benkhaled, G. Volpi, V. Lapinte and S. Blanquer, *Mater. Adv.*, 2024, **5**, 2750–2758.
12 A. Rath, P. Geethu, S. Mathesan, D. K. Satapathy and P. Ghosh, *Soft Matter*, 2018, **14**, 1672–1680.
13 P. Lv, X. Yang, H. K. Bisoyi, H. Zeng, X. Zhang, Y. Chen, P. Xue, S. Shi, A. Priimagi and L. Wang, *et al.*, *Mater. Horiz.*, 2021, **8**, 2475–2484.
14 V. Kumar and D. K. Satapathy, *Langmuir*, 2024, **40**, 11206–11214.
15 A. Dallinger, P. Kindlhofer, F. Greco and A. M. Coclite, *ACS Appl. Polym. Mater.*, 2021, **3**, 1809–1818.
16 G. Manikandan, A. Murali, R. Kumar and D. K. Satapathy, *ACS Appl. Mater. Interfaces*, 2021, **13**, 8880–8888.
17 J. P. Serra, L. C. Fernandes, D. M. Correia, C. R. Tubio, J. L. Vilas-Vilela, M. Tariq, J. M. Esperança, C. M. Costa and S. Lanceros-Mendez, *Mater. Adv.*, 2022, **3**, 937–945.
18 V. Kumar and D. K. Satapathy, *Soft Matter*, 2024, **20**, 5435.
19 M. Ganesan, R. Kumar and D. K. Satapathy, *Langmuir*, 2022, **38**, 6066–6075.
20 W. Wang, Y.-L. Zhang, B. Han, J.-N. Ma, J.-N. Wang, D.-D. Han, Z.-C. Ma and H.-B. Sun, *Sens. Actuators, B*, 2019, **290**, 133–139.
21 L. Zhang, P. Naumov, X. Du, Z. Hu and J. Wang, *Adv. Mater.*, 2017, **29**, 1702231.
22 H. Deng, Y. Dong, C. Zhang, Y. Xie, C. Zhang and J. Lin, *Mater. Horiz.*, 2018, **5**, 99–107.
23 H. Chathuranga, I. Marriam, S. Chen, Z. Zhang, J. MacLeod, Y. Liu, H. Yang and C. Yan, *ACS Appl. Mater. Interfaces*, 2022, **14**, 16772–16779.
24 L. Zheng, H. Li, W. Huang, X. Lai and X. Zeng, *ACS Appl. Mater. Interfaces*, 2021, **13**, 36621–36631.
25 K. Feng, G. Wei, Y. Liu, Y. Wu and F. Zhou, *ACS Sustainable Chem. Eng.*, 2023, **11**, 8374–8385.
26 Y. Liu, X.-C. Sun, C. Lv and H. Xia, *Smart Mater. Struct.*, 2021, **30**, 125014.
27 A. Kumar, R. Rajamanickam, J. Hazra, N. R. Mahapatra and P. Ghosh, *ACS Appl. Mater. Interfaces*, 2022, **14**, 56321–56330.
28 Y. Wang, Z. Wang, Z. Lu, M. Jung de Andrade, S. Fang, Z. Zhang, J. Wu and R. H. Baughman, *ACS Appl. Mater. Interfaces*, 2021, **13**, 6642–6649.
29 X. Wang, Z. Bai, M. Zheng, O. Yue, M. Hou, B. Cui, R. Su, C. Wei and X. Liu, *J. Sci.: Adv. Mater. Devices*, 2022, **7**, 100451.
30 Y. Kuang, C. Chen, J. Cheng, G. Pastel, T. Li, J. Song, F. Jiang, Y. Li, Y. Zhang and S.-H. Jang, *et al.*, *Extreme Mech. Lett.*, 2019, **29**, 100463.
31 Z. Zhao, Y. Hwang, Y. Yang, T. Fan, J. Song, S. Suresh and N.-J. Cho, *Proc. Natl. Acad. Sci. U. S. A.*, 2020, **117**, 8711–8718.
32 H. Chathuranga, I. Marriam, Z. Zhang, J. MacLeod, Y. Liu, H. Yang and C. Yan, *Adv. Mater. Technol.*, 2022, **7**, 2100447.
33 M. Gómez-Guillén, B. Giménez, M. A. López-Caballero and M. Montero, *Food Hydrocolloids*, 2011, **25**, 1813–1827.
34 D. Liu, M. Nikoo, G. Boran, P. Zhou and J. M. Regenstein, *Annu. Rev. Food Sci. Technol.*, 2015, **6**, 527–557.
35 J. Poppe, *Thickening and gelling agents for food*, 1992, pp. 98–123.
36 L. G. Gonzalez and T. J. Wess, *Heritage Sci.*, 2013, **1**, 1–8.
37 S. Yang, Y. Zhang, T. Wang, W. Sun and Z. Tong, *ACS Appl. Mater. Interfaces*, 2020, **12**, 46701–46709.
38 J. Huang, L. Zhao, T. Wang, W. Sun and Z. Tong, *ACS Appl. Mater. Interfaces*, 2016, **8**, 12384–12392.
39 Y. Zhu, L. Lin, Y. Chen, Y. Song, W. Lu and Y. Guo, *Soft Matter*, 2020, **16**, 2238–2248.
40 J. Muyonga, C. Cole and K. Duodu, *Food Chem.*, 2004, **85**, 81–89.
41 T. Aewsiri, S. Benjakul and W. Visessanguan, *Food Chem.*, 2009, **115**, 243–249.
42 F. Badii, W. MacNaughtan, J. Mitchell and I. Farhat, *Drying Technol.*, 2014, **32**, 30–38.
43 A. Bigi, S. Panzavolta and K. Rubini, *Biomaterials*, 2004, **25**, 5675–5680.
44 I. Yakimets, N. Wellner, A. C. Smith, R. H. Wilson, I. Farhat and J. Mitchell, *Polymer*, 2005, **46**, 12577–12585.
45 M. Rahman, K. Dey, F. Parvin, N. Sharmin, R. A. Khan, B. Sarker, S. Nahar, S. Ghoshal, M. Khan and M. M. Billah, *et al.*, *Int. J. Polym. Mater.*, 2011, **60**, 1056–1069.
46 F. Liu, H. Majeed, J. Antoniou, Y. Li, Y. Ma, W. Yokoyama, J. Ma and F. Zhong, *Food Hydrocolloids*, 2016, **58**, 20–28.

© 2024 The Author(s). Published by the Royal Society of Chemistry

Open Access Article. Published on 05 August 2024. Downloaded on 2/21/2026 9:32:34 AM.
This article is licensed under a Creative Commons Attribution-NonCommercial 3.0 Unported Licence.

47 G. Aguirre-Alvarez, D. Pimentel-González, R. Campos-Montiel, T. Foster and S. Hill, *CyTA–J. Food*, 2011, **9**, 243–249.
48 K. Zhang, A. Geissler, M. Standhardt, S. Mehlhase, M. Gallei, L. Chen and C. Marie Thiele, *Sci. Rep.*, 2015, **5**, 1–13.
49 L. Chen, M. Weng, P. Zhou, L. Zhang, Z. Huang and W. Zhang, *Nanoscale*, 2017, **9**, 9825–9833.
50 L. Zhang, Y. Zhang, F. Li, S. Yan, Z. Wang, L. Fan, G. Zhang and H. Li, *ACS Appl. Mater. Interfaces*, 2019, **11**, 12890–12897.
51 Y. Gu, X. Huang, C. G. Wiener, B. D. Vogt and N. S. Zacharia, *ACS Appl. Mater. Interfaces*, 2015, **7**, 1848–1858.
52 H. Yu, C. Peng, F.-C. Li and P. Yu, *Mater. Res. Express*, 2019, **6**, 126414.
53 P. Hazaveh, A. M. Nafchi and H. Abbaspour, *Int. J. Biol. Macromol.*, 2015, **79**, 370–376.
54 B. Fauziyah, D. Fatimatussholichah, A. R. Syarifah and B. Ma'arif, *J. Adv. Pharm. Technol. Res.*, 2023, **14**, 56.
55 P. Kozlov and G. Burdygina, *Polymer*, 1983, **24**, 651–666.
56 J. Bella, M. Eaton, B. Brodsky and H. M. Berman, *Science*, 1994, **266**, 75–81.
57 J. Bella, B. Brodsky and H. M. Berman, *Structure*, 1995, **3**, 893–906.
58 R. W. Kugel, *J. Chem. Educ.*, 1998, **75**, 1125.